Carbon 98 (2016) 666–670

Contents lists available at ScienceDirect

Carbon

journal homepage: www.elsevier.com/locate/carbon

Local property change of graphene induced by a Cu nanoparticle

Li-Wei Huang [a, b, c], Horng-Tay Jeng [a, d], Cheng-Kai Chang [e, f], Kuei-Hsien Chen [e], Fu-Rong Chen [b], Chia-Seng Chang [a, c, *]

[a] Institute of Physics, Academia Sinica, Taipei 11529, Taiwan, ROC
[b] Department of Engineering and System Science, National Tsing Hua University, Hsinchu 30013, Taiwan, ROC
[c] Nano Science and Technology Program, Taiwan International Graduate Program, Academia Sinica and National Tsing Hua University, Taiwan, ROC
[d] Department of Physics, National Tsing Hua University, Hsinchu 30013, Taiwan, ROC
[e] Institute of Atomic and Molecular Sciences, Academia Sinica, Taipei 10617, Taiwan, ROC
[f] Institute of Polymer Science and Engineering, National Taiwan University, Taipei 10617, Taiwan, ROC

ARTICLE INFO

Article history:
Received 9 July 2015
Received in revised form
23 November 2015
Accepted 25 November 2015
Available online 30 November 2015

ABSTRACT

Investigating the detailed impact from an individual nanoparticle on a graphene membrane is a great challenge. We employed ultra-high vacuum electron microscopy and first-principles calculations to reveal the changes in graphene morphology and electronic structure when in contact with a Cu nanoparticle. Our findings show that the significant amount of charge transfer from the individual Cu nanoparticle to graphene causes local electronic redistributions at the interface and a consequent recess of the graphene with prominent tilt angles.

1. Introduction

Understanding how an individual metal nanoparticle interacts with a graphene membrane lays the foundation for further exploring and exploiting the associated extraordinary properties of this system. Many of the proposed phenomena and applications with graphene involve the presence of metal nanoparticles, and their combination may thus be viewed as a new type of functional material [1–3]. Free-standing graphene is also known as an ultimate support for transmission electron microscopy (TEM) samples [4] because its periodic lattice of carbon atoms renders chemical inertness and structural stability along with high electron transparency. Even so, the inevitable interaction between the sample and substrate could perturb the intrinsic properties of the sample. Small particles imaged by high resolution TEM can be dated back to 1980's [5] and the Wulff construction has been proposed to interpret their structures. TEM has also been employed to study the interface energetics of Ag nanocrystals on a H-passivated Si(111) surface, and it was found that the interface energy minimum, which determines the equilibrium orientation, depended on the interface size and shape [6].

In this paper, we use the ultra-high vacuum (UHV, base pressure 2×10^{-10} torr) high-resolution TEM (HR-TEM) and first-principles calculations to investigate the structural deformation of a suspended graphene sheet beneath an adsorbed copper (Cu) nanoparticle. Our motivation has been, on one hand, most chemical vapor deposition (CVD) grown graphene uses Cu foils as the substrate and the Cu residues are often found after the transferring process. On the other hand, hybrid materials of Cu and carbon have attracted considerable interests in catalytic enhancement, applications in photo-electrochemical devices, materials of transparent conductive electrode, and more [7–10]. Our findings indicate that the icosahedral Cu nanoparticle adheres to the graphene with two adjacent (111) facets. The C–C bond lengths of graphene underneath the Cu nanoparticle are significantly elongated owing to the local electron charge transfer from Cu to graphene, which results in subsequent nearby property changes of the graphene.

2. Experimental

Graphene used in the current study was grown on 25 μm thick Cu foil (Alfa Aesar, 99.8% purity) by the CVD method [11,12]. Suspended graphene samples were obtained by transferring the CVD grown graphene from copper foils to TEM copper grids [13]. We then fabricate the clean graphene by annealing the sample to 700 °C under 10^{-5} torr H_2 environment to eliminate PMMA, amorphous carbon and residual Cu on graphene surface [14]. In-

* Corresponding author. Institute of Physics, Academia Sinica, Taipei 11529, Taiwan, ROC
E-mail address: jasonc@phys.sinica.edu.tw (C.-S. Chang).

http://dx.doi.org/10.1016/j.carbon.2015.11.064
0008-6223/

situ deposition of high purity metal atoms (Cu, 99.99%, Nilaco) onto the suspended graphene was carried out in the same UHV-TEM chamber with a highly collimated e-beam evaporator. Cu atoms of 0.01 monolayer (ML) coverage were deposited onto graphene under the pressure of 2×10^{-8} torr and Cu nanoparticles were formed by agglomeration at room temperature. To avoid the radiation damage during the TEM investigation, we used the electron beam of 100 kV at a low dose rate of ~1200 electrons nm^{-2} sec^{-1} [15].

The electronic structure calculations were performed using the full-potential projected augmented wave method [16,17] as implemented in the Vienna ab-initio simulation package (VASP) [18,19] within the local density approximation. To simulate the Cu cluster/graphene system, we use a 6×6 supercell of graphene with a pyramidal Cu cluster and a vacuum thickness over 15 Å, as shown in Fig. 3(3a and 3b). The Cu cluster contains 11 Cu atoms with seven in the basal plane of the pyramid contacting the graphene, three atoms in the middle plane, and one Cu atom at the tip of the pyramid. Cu atoms in the basal plane situate at the hollow site of the graphene honeycomb structure. We have also done calculations for Cu clusters with different sizes located at both the top site and hollow site and the results show no significant difference. The geometry of the considered systems is optimized with the total energies converged within 0.001 eV/cell. The self-consistent calculations and the geometry optimization are performed on a $6 \times 6 \times 1$ Monkhorst-Pack k-point mesh (20 k-points) with the cutoff energy of 400 eV.

3. Results and discussion

The interactions of metal clusters with graphene sheets are not yet fully understood, mainly due to the serious obstruction and disturbance of contaminations on graphene surface. Huang et al. [14] recently demonstrated a method to fabricate a large area of clean graphene, which provides a perfect starting ground to study the intrinsic interaction between a metal nanoparticle and graphene. A representative bright field (BF) TEM image of a clean graphene membrane of 250×250 nm is shown in the supplemental materials Fig. S1, where the atomic cleanness and the lattice of graphene sample are easily verified. We used HREM, fast Fourier transfer (FFT), inversed FFT (IFFT) and centered dark-field (CDF) techniques to reveal the detailed interfacial structure between the graphene and Cu nanoparticle. Fig. 1a shows the atomically resolved BF TEM image of the suspended graphene supporting the most perfect icosahedral Cu nanoparticle with twins and facets. The multiply-twinned icosahedron structure assumed by the Cu nanoparticle is most typical, consisting of twenty tetrahedral subgrains, thirty edges, twelve vertices and twenty {111} faces [5,20], as a detailed image in the Supplemental Information Fig. S2. The isolated imaging technique was performed to remove the structure of Cu nanoparticle from the HREM image in order to reveal the underneath graphene structure [21]. An FFT of only graphene membrane, as shown in Fig. 1b, was taken from the area indicated by the red box in the Fig. 1a, exhibiting hexagonal spot patterns that are characteristic of graphene. The other FFT of graphene sheet and the Cu nanoparticle, as shown in Fig. 1c, was taken from the entire area of Fig. 1a. Deflections from the graphene and Cu nanoparticle are clearly distinguishable by comparing the FFT digital diffractogram of Fig. 1b with that of Fig. 1c. The interface between the graphene and Cu nanoparticle can be made visible by subtracting the deflection from Cu nanoparticle in Fourier space. Fig. 1d, an IFFT image, shows a clear footprint of the Cu nanoparticle on the graphene membrane. A dark-field imaging (Fig. 1e) is formed via collecting the [0–110] deflection beam of graphene in the CDF mode [22]. The rhombic region of high intensity (bright area) represents where the stronger scattering occurs owing to higher electron density of this area, doped by the Cu nanoparticle. The rhombic shape comprises two triangular (111) facets of the Cu nanoparticle, which is illustrated by the two triangles delineated by red dashed lines in the inset of Fig. 1e.

The nano-beam electron diffraction (NBD) measurement has been applied to evaluate the subtle variation of bond length [23–25]. We also use this technique to investigate the direct structural impact of an individual Cu nanoparticle on a suspended graphene. The size of the NBD probe for 100 kV is 4.5 nm in diameter with intensity profile shown in Supplemental Information Fig. S3, which allows us to obtain the diffraction pattern from a small region to acquire the subtle deformation of local bond-length. Fig. 2a shows the BF TEM image of graphene sheet with a Cu nanoparticle (8.5 nm in diameter). The corresponding NBD patterns Fig. 2(c to i) were obtained at seven consecutive positions from the bottom left to the top right as indicated by respective color circles in Fig. 2a. The NBD patterns of graphene exhibit six primary deflections along [0–110], reflecting the hexagonal symmetry with the periodicity of 2.13 Å spacing of the pristine lattice [26]. We quantified the variations of this spacing in real space by measuring the distance between graphene diffraction spots (01–10) and (0–110), denoting as 2R, for each NBD pattern in the images from Fig. 2(c to i). This 2R increases under the Cu nanoparticle, but in real space this means the lattice spacing projected normal to the e-beam direction, defined as χ, actually decreases. With careful measurements shown in the Supplemental Information Figs. S4–S6, we plot the resultant variations of χ on seven consecutive positions in Fig. 2b as A = 0%, B = 0%, C = −1.50%, D = −3.75%, E = −1.50%, F = 0%, G = 0%. The variations reflect the scale of interaction between the Cu nanoparticle and the graphene

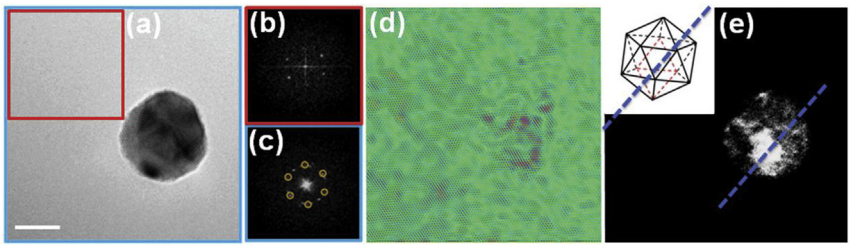

Fig. 1. Characteristics of graphene-Cu nanoparticle interface (a) The HRTEM atomic-resolution image of suspended graphene with the twinned and faceted Cu icosahedral nanoparticle, scale bar = 5 nm. (b) Digital diffractogram of the graphene membrane taken from the region in (a) indicated by red box. (c) Digital diffractrogram of the graphene membrane and Cu nanoparticle taken from the region in (a) indicated by blue box. (d) The IFFT image generated by only selecting graphene diffraction spots in (c) indicated by yellow rings for the subtraction of Cu nanoparticle reflections to see the interface. (e) A CDF image recorded via an graphene (0–110) diffraction spot, displaying the Cu nanoparticle contacting graphene with two adjacent triangular facets forming a rhombic shape, which also illustrated by red dashed line in the inset. (A colour version of this figure can be viewed online.)

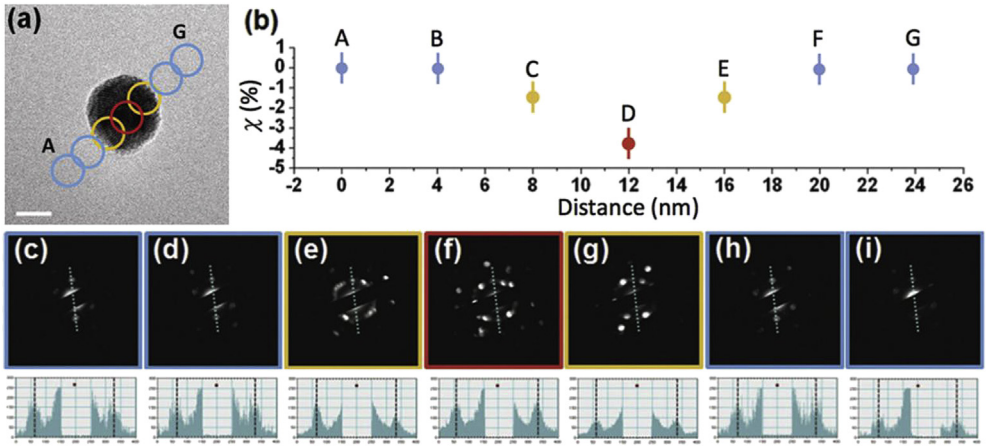

Fig. 2. (a) The TEM image illustrating consecutive measurement positions of NBD (probe size = 4.5 nm) on the suspended graphene membrane with colored rings, scale bar = 5 nm. (b) Corresponding NBD measurements to consecutive colored circular area in (a) indicating differences of graphene bonding length projections of [0–110] periodicity, χ. (c) to (i) illustrated the measurement of differences of [0–110] projections, χ, corresponding to colored points A to G in (b) from left to right, A = 0%, B = 0%, C = −1.50%, D = −3.75%, E = −1.50%, F = 0%, G = 0%, error bar = ± 0.75%. (A colour version of this figure can be viewed online.)

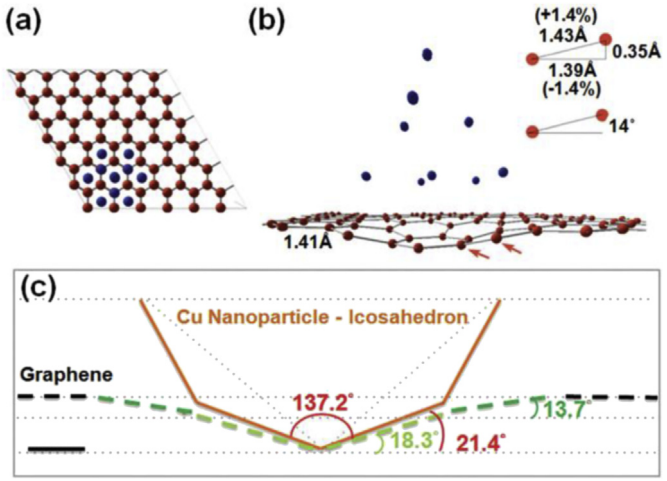

Fig. 3. Top view (a) and 3-dimensional plot (b) of the optimized structure of Cu cluster/graphene 6 × 6 lattice. Red and blue spheres are C and Cu atoms, respectively. Upright inset in (b) showing local structure of the distorted C–C bond as indicated by red arrows. (c) The sketch illustrates the recess on graphene coping with the facets of Cu icosahedron. (A colour version of this figure can be viewed online.)

membrane, which is concentrated around the Cu nanoparticle.

We performed the first principles calculations on the geometric optimization of a simplified Cu pyramid/graphene model system to elicit the origin of this interaction. Fig. 3(a and b) depicts both the top view and 3-dimensional plot of the optimized structure of our model system. The lattice distortion of the honeycomb structure beneath the Cu cluster can be clearly seen. The major distortions include 1) the elongation of the C–C bond length from 1.41 Å at the Cu-free region to 1.43 Å (~1.4% longer) at the Cu–C interface; 2) an outward tilting angle of ~14° at the Cu–C interface resulted from the stretch of C–C bond on the graphene, as evidenced in Fig. 3b. Combining these two geometrical distortions together, the projection of the elongated C–C bond onto the a-b plane is actually ~1.4% shorter (1.39 Å, as seen in the inset of Fig. 3b) than the unaffected bond length of 1.41 Å, qualitatively agreeing with our experimental observation on shrinkage of the C–C bond derived from the diffraction pattern.

We have further calculated the band structures and density of states to seek the cause of C–C bond elongation in this system. As plotted in Fig. 4a, the nearly double-degenerated Dirac cone

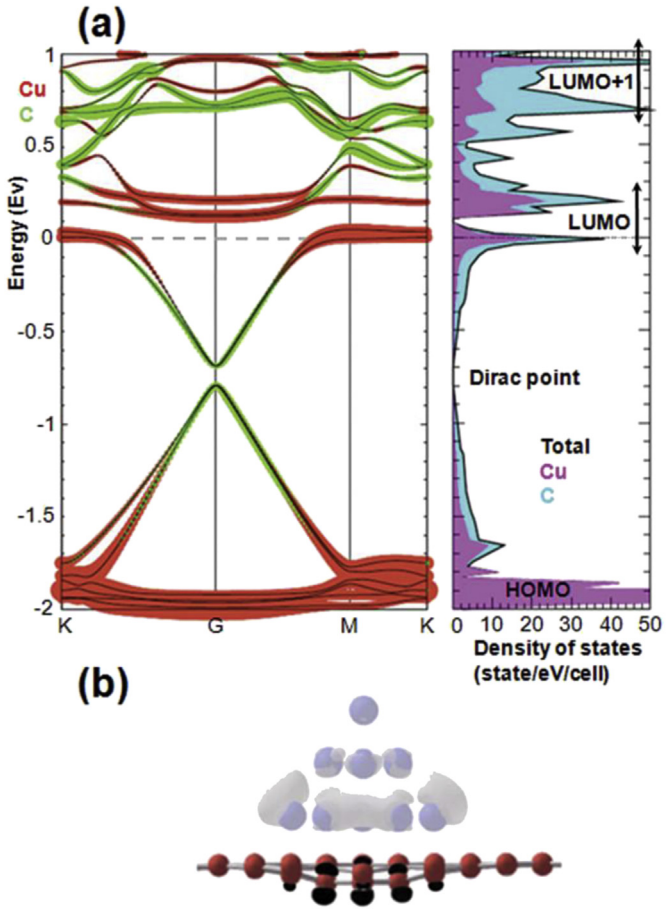

Fig. 4. (a) Left panel, site-decomposed band structures of Cu/graphene. The sizes of red and green spheres indicate contributions from Cu and C atoms at the contact area. The right panel of (a) shows the total density of states (black) and projections onto Cu (magenta) and C (cyan) atoms. HOMO and LUMO indicate the highest occupied molecular orbital and the lowest unoccupied molecular orbital of the Cu pyramid, respectively. (b) The extra electron (black) distribution over the graphene membrane and the hole distribution (gray) over the Cu cluster. (A colour version of this figure can be viewed online.)

significantly sinks into the Fermi sea by about 0.7 eV with about 50% of the Dirac cone area at the Fermi level occupied, corresponding to ~2e/cell (~2e/72C atoms) charge transfer from the Cu cluster to the graphene. The amount is more or less compatible to the huge charge transfer of ~3e/60C found in the system of C_{60} absorbed on the bulk Cu(111) surface [27]. Both the large amount of charge received by graphene and pronounced band shift of the Dirac cone greatly enhance the C–C bond length, reflecting the strong interaction between Cu and C atoms. This strong Cu–C interaction further opens up an energy gap of about 0.1 eV at the Dirac point. Notice that this sizeable energy gap at the Dirac point in this system could be a new avenue towards the gap-manipulation of graphene, which is highly desirable for industrial applications based on graphene [28–30].

The density of states (Fig. 4a) also demonstrates the band gap at the Dirac point and the electron-doped graphene from the exhausted Cu-4s bands above the Fermi level. Since all the observed phenomena can be traced back to the same origin: the large amount of charge transfer from the Cu cluster to the graphene, we further explore the spatial distribution of this charge transfer. Fig. 4b demonstrates the distribution of the extra electron (black) over the graphene membrane. As shown, all these extra electrons doped onto the out-of-plane C-pi bonds of the C atoms beneath the Cu cluster, whereas the electron cloud diminishes quickly out of the Cu cluster (displayed in grey). Take this localized electron picture into consideration, the ~2e/cell charge transfer mainly distributes over about 18C atoms beneath the Cu pyramid, therefore the effective charge transfer would be as high as ~0.11e/C. We have also done calculations for scaling in the Cu cluster size and the results show the size of the Cu–C contacting area rather than the size of Cu cluster plays the key role on the total charge transfer. As the contacting area is over 7Cu, the charge transfer per Cu atom is then excellently saturate at the value of 0.1e/C, more details as shown in supplemental materials Table S1. While in the C_{60}/Cu(111) system [27], the ~3e/60C charge transfer locates mostly at the lower half of C_{60}, which corresponds to 0.1e/C. The good agreement between these two systems indicates the large amount of charge transfer ~0.1e/C could be generic at the Cu–C contact and not size sensitive.

Experimentally, the contact structure between the Cu nanoparticle and graphene is found more complicated, which usually involves more than one (111) facet. In rare occasions we can obtain a discernable image of the contact as that shown in Fig. 1(e). At this contact, the major driving force is to induce maximum charge transfer from the Cu to C atoms while the elastic energy is responsively stored in the graphene lattice due to the structural distortion. So, the overall morphological deformation of the graphene sheet is expected closely related to the contact structure. According to the simulation above, we can now quantitatively explain our NDB results displayed in Fig. 2. The local electron-doped graphene extended its C–C bond to 1.43 Å (~1.4% from the original $d = 1.41$ Å). Since this local bond stretch is caused by the generic ~0.1e/C charge transfer between Cu and C atoms, we assume the C–C bond length under the Cu nanoparticle also takes up this value. Now to resolve our experimental findings for projected bond-length shrinkage, referring to Fig. 2(b), i.e. at C point −1.5% and D point −3.75%, we need to dip the graphene lattice underneath the Cu by $\cos^{-1}(0.985d/1.014d) = 13.7^\circ$ and $\cos^{-1}(0.9625d/1.014d) = 18.3^\circ$, respectively. The whole picture is illustrated in Fig. 3c. The recess formed on the graphene fits well with the two adhering (111) facets of Cu icosahedron that have a dihedral angle of 137.2° and 21.4° to the horizontal. The concave shape of the recess to match the two facets seems to incur for maximum electron charge transfer from the Cu icosahedron to graphene membrane.

4. Conclusions

We have resolved the significant charge transfer from a Cu nanoparticle to graphene as the origin of local C–C bond length elongation. The structural deformation of graphene underneath a Cu icosahedron has been quantitatively observed and measured. Our first-principles calculations also indicate a likely generic electron transfer between Cu and C atoms, which can induce a sizable gap opening at the graphene Dirac point.

Acknowledgements

The authors would like to thank Tung Hsu for fruitful discussion. This work was supported by the Taiwan National Science Council under grant number NSC 101-2112-M-001-022-MY3. H.T.J. is supported by the National Science Council, Taiwan and thanks NCHC, CINC–NTU and NCTS, Taiwan for technical support.

Appendix A. Supplementary data

Supplementary data related to this article can be found at http://dx.doi.org/10.1016/j.carbon.2015.11.064.

References

[1] G. Giovannetti, P.A. Khomyakov, G. Brocks, V.M. Karpan, J. van den Brink, P.J. Kelly, Doping Graphene with Metal Contacts, Phys. Rev. Lett. 101 (2008) 026803–026804.
[2] A.V. Krasheninnikov, P.O. Lehtinen, A.S. Foster, P. Pyykkö, R.M. Nieminen, Embedding Transition-Metal Atoms in Graphene: Structure, Bonding, and Magnetism, Phys. Rev. Lett. 102 (2009), 126807-4.
[3] S.S. Carara, R.J.C. Batista, H. Chacham, Modifications in graphene electron states due to a deposited lattice of Au nanoparticles: density functional calculations, Phys. Rev. B 80 (2009) 115435–115437.
[4] J.C. Meyer, C.O. Girit, M.F. Crommie, A. Zettl, Imaging and dynamics of light atoms and molecules on graphene, Nature 454 (2008) 319–322.
[5] L.D. Marks, Imaging small particles, Ultramicroscopy 18 (1985) 445–452.
[6] J.K. Bording, B.Q. Li, Y.F. Shi, J.M. Zuo, Size- and shape-dependent energetics of nanocrystal interfaces: experiment and simulation, Phys. Rev. Lett. 90 (22) (2003), 226104–4.
[7] P. Mondal, A. Sinha, N. Salam, A.S. Roy, N.R. Jana, S.M. Islam, Enhanced catalytic performance by copper nanoparticle–graphene based composite, RCS Adv. 3 (2013) 5615–5623.
[8] M. Scarselli, P. Castrucci, L. Camilli, S.D. Gobbo, S. Casciardi, F. Tombolini, et al., Influence of Cu nanoparticle size on the photo-electrochemical response from Cu–multiwall carbon nanotube composites, Nanotechnology (2011) 22, 035701.
[9] L. Jiang, X. Lu, X. Zheng, Copper/silver nanoparticle incorporated graphene films prepared by a low-temperature solution method for transparent conductive electrodes, J. Mater Sci. Mater Electron 25 (2014) 174–180.
[10] X. Li, W. Cai, L. Colombo, R.S. Ruoff, Evolution of graphene growth on Ni and Cu by carbon isotope labeling, Nano Lett. 9 (12) (2009) 4268–4272.
[11] X. Li, W. Cai, J. An, S. Kim, J. Nah, D. Yang, et al., Large-area synthesis of high-quality and uniform graphene films on copper foils, Science 324 (2009) 1312–1314.
[12] J.Y. Hwang, C.C. Kuo, L.C. Chen, K.H. Chen, Correlating defect density with carrier mobility in large-scaled graphene films: Raman spectral signatures for the estimation of defect density, Nanotechnology 21 (2010) 465705.
[13] X. Li, Y. Zhu, W. Cai, M. Borysiak, B. Han, D. Chen, et al., Transfer of large-area graphene films for high-performance transparent conductive electrodes, Nano Lett. 9 (12) (2009) 4359–4363.
[14] L.W. Huang, C.K. Chang, F.C. Chien, K.H. Chen, P. Chen, F.R. Chen, et al., Characterization of the cleaning process on a transferred graphene, J. Vac. Sci. Technol. A 32 (5) (2014) 050601–050605.
[15] Z. Liu, K. Suenaga, P.J.F. Harris, S. Iijima, Open and closed edges of graphene Layers, Phys. Rev. Lett. 102 (2009) 015501–015504.
[16] P.E. Blöchl, Projector augmented-wrave method, Phys. Rev. B 50 (24) (1994) 17953–17979.
[17] G. Kresse, D. Joubert, From ultrasoft pseudopotentials to the projector augmented-wave method, Phys. Rev. B 59 (3) (1999) 1758–1775.
[18] G. Kresse, J. Hafner, Ab initio molecular dynamics for open-shell transition metals, Phys. Rev. B 48 (17) (1993) 13115–13118.
[19] G. Kresse, J. Furthmüller, Efficient iterative schemes for ab initio total-energy calculations using a plane-wave basis set, Phys. Rev. B 54 (16) (1996) 11169–11186.
[20] L.D. Marks, D.J. Smith, High resolution studies of small particles of gold and silver, J. Cryst. Growth 54 (1981) 425–432.

[21] Z. Lee, K.J. Jeon, A. Dato, R. Erni, T.J. Richardson, M. Frenklach, et al., Direct imaging of soft-hard interfaces enabled by graphene, Nano Lett. 9 (9) (2009) 3365–3369.
[22] D.B. Williams, C.B. Carter, Transmission Electron Microscopy: a Textbook for Materials Science, second ed., Springer, New York, 2009.
[23] F.H. Baumann, High precision two-dimensional strain mapping in semiconductor devices using nanobeam electron diffraction in the transmission electron microscope, Appl. Phys. Lett. 104 (2014) 262102–262104.
[24] D. Cooper, A. Béché, J.M. Hartmann, V. Carron, J.L. Rouvi'ere, Strain mapping for the semiconductor industry by dark-field electron holography and nanobeam electron diffraction with nm resolution, Semicond. Sci. Technol. (2010) 25, 095012.
[25] K. Usuda, T. Numata, T. Irisawa, N. Hirashita, S. Takagi, Strain characterization in SOI and strained-Si on SGOI MOSFET channel using nano-beam electron diffraction (NBD), Mater Sci. Eng. B 124 (2005) 143–147.
[26] J.C. Meyer, A.K. Geim, M.I. Katsnelson, K.S. Novoselov, T.J. Booth, S. Roth, The structure of suspended graphene sheets, Nature 446 (2007) 60–63.
[27] W.W. Pai, H.T. Jeng, C.M. Cheng, C.H. Lin, X. Xiao, A. Zhao, et al., Optimal electron doping of a C_{60} monolayer on Cu(111) via interface reconstruction, Phys. Rev. Lett. 104 (2010) 036103–036104.
[28] C.K. Chang, S. Kataria, C.C. Kuo, A. Ganguly, B.Y. Wang, J.Y. Hwang, et al., Band gap engineering of chemical vapor deposited graphene by in situ BN doping, ACS Nano 7 (2) (2013) 1333–1341.
[29] A.J. Samuels, J.D. Carey, Molecular doping and band-gap opening of bilayer graphene, ACS Nano 7 (3) (2013) 2790–2799.
[30] M.Y. Han, B. Özyilmaz, Y. Zhang, P. Kim, Energy band-gap engineering of graphene nanoribbons, Phys. Rev. Lett. 98 (2007), 206805–4.